ARTICLES

Functionalized Nanoparticle Films with Rectifying Conduction Properties

Torsten Reda*,† and Anthony F. Collings

CSIRO Telecommunications & Industrial Physics, P.O. Box 218, Lindfield, NSW 2070, Australia

Chris Barton and Philip Lukins

School of Physics, University of Sydney, Sydney, NSW 2006, Australia

Received: April 1, 2003; In Final Form: August 26, 2003

Gold and silver nanoparticles functionalized at their surfaces with electron acceptor (TCNQ) and donor (TMPD) molecules were spray-deposited as thin films on highly ordered pyrolytic graphite (HOPG) substrates. Pure films and bilayer structures were investigated by means of scanning tunneling spectroscopy (STS). The pure films show symmetric current−voltage dependences, whereas the bilayer structures are characterized by a diode-like behavior with rectification ratios of up to 66 at ±75 mV for structures containing silver nanoparticles and 6.5 at ±1 V for analogous structures based on gold nanoparticles. Such properties have been previously described for molecular rectifiers containing electron acceptor and donor groups. Our results suggest that electronic structures of this type might be assembled alternatively through appropriate nanoscale architectures using sequential deposition of functionalized nanoparticles.

1. Introduction

The development of electronic devices beyond the limitation of conventional photolithographic techniques is seen as a significant step toward controlling physical matter in nanometer dimensions. To reach this goal, active and passive components must be extremely small with diameters no larger than several nanometers corresponding to not more than a few molecules of medium molecular weight. As a result, molecules become the focus of intensive investigations with respect to their electronic, optoelectronic, and chemoelectronic properties. Additionally, the question of how to assemble molecules into larger 2- and 3-D structures becomes more relevant. Complex molecular systems will not totally self-assemble, nor can they be grafted, step-by-step, by robotic machines which have positional accuracies of molecular dimensions. Success will probably require a combination where chemical reactions are steered in compartments which are separated in space and time by manipulators operating on submicron length scales.

Despite the inherent difficulties, remarkable results have been achieved in molecular electronics. Following Aviram and Ratner[1] who predicted theoretically single molecules with rectifying electrical properties, the groups of Ashwell and Sambles[2,3] as well as Metzger[4,5] subsequently proved that donor-(D)−bridge−acceptor(A) compounds indeed showed such diode behavior. The earlier measurements concerned metal/Langmuir−Blodgett (LB) film/metal structures with top electrodes made from metals with low sublimation temperatures. Those might have formed oxide layers which interfere with the current−voltage behavior of the sandwiched molecular structures. Recent work has produced non-oxidizing gold/LB film/gold devices probing undisputable the molecular rectifying properties of D−bridge−A compounds.[6−12] Other type molecules have demonstrated slightly asymmetric current−voltage characteristics[13] or reversible switching properties with relatively large on−off ratios of up to 1000:1.[14]

Compared with such single-molecule devices, there are many examples of structures which exploit hetero-molecular contacts or soft matter solid-state interfaces without connecting covalent bonds. Electrically conducting organic crystals,[15] field-effect transistors,[16] and organic light-emitting diodes (OLED)[17] are such examples. OLEDs employ thin films of electron transport layers, organic emitters, and hole injection layers to create a light-emitting interface. Even though the molecules are not chemically linked in this case, they are electronically coupled. To date, there are no measurements which conclusively indicate qualitative differences in electron-transfer rates for systems connected via chemical bonds compared to other bonding forces.

It becomes more difficult to experimentally investigate hetero-molecular interfaces as they become thinner. It is usually difficult to align organic materials densely packed in ultrathin films. Structural defects combined with common problems of smoothly applying an appropriate second electrode have meant that hetero-molecular devices are relatively rare. Fischer et al. produced de facto bimolecular rectifiers by fabricating LB film-based gold/metallophthalocyanine/perylene/gold structures.[18,19] The working samples contained 6 layers of each, respectively, of the organic compounds, and sophisticated vacuum metal deposition was used to mount the top electrode. Another example is the contact of two self-assembled monolayers, whereby one contact has been realized via a soft mercury electrode.[20]

* Corresponding author. E-mail: tr@mrc-dunn.cam.ac.uk.

† Current address: Torsten Reda, MRC Dunn Human Nutrition Unit, Hills Road, Cambridge CB2 2XY, U.K. Telephone: +44-1223 252810. Fax: +44-1223 252815. E-mail: tr@mrc-dunn.cam.ac.uk.

10.1021/jp034836a CCC: $25.00
Published on Web 11/22/2003

Rather than using LB-based techniques, we have produced films based on surface-modified nanoparticles. Our proposition is that any thiol or disulfide can be used to functionalize gold or silver nanoparticles via thiolate bonds.[21−23] Furthermore, the large surface energies of nanometer-sized particles promote effective binding of other organic materials which contain, for example, nitrogen, aromatic and hetero-aromatic rings, charged functional groups, and so on. Such functionalized nanoparticles can be utilized to form layered or interdigital structures by absorption,[24] spray deposition, and printing.[25] Thus, heteromolecular interfaces are created when different types of nanoparticles or, more correctly, their functionalized surfaces, are in close contact. If the nanoparticles are metallic they will act as a conductive backbone. This approach could be used to assemble nanoscale devices by creating asymmetric interfaces between chemical compounds without necessarily linking them via covalent bonds. The present work shows how heteromolecular interfaces between electron donors and acceptors of respectively functionalized nanoparticles form a rectifier.

2. Experimental Details

Aqueous solutions of sodium citrate-coated gold nanoparticles of approximately 15 nm diameter were made by the method of Turkevich[26] and Frens.[27] Yellow silver colloids ca. 10 nm in diameter were prepared by a method based on that reported by Creighton et al.[28] through the reduction of $AgNO_3$ by $NaBH_4$. Grey silver colloids ca. 80 nm in diameter were prepared as described by Lee and Meisel,[29] again using sodium citrate as the reducing and stabilizing agent for the colloidal solution. All chemicals and solvents were obtained from Sigma-Aldrich or Fluka and used without further purification. Milli-Q water was used.

2.1. Preparation of Functionalized Nanoparticle Concentrates. Solutions (100 mM) of 7,7,8,8-tetracyano-*p*-quinodimethane (TCNQ), *N*,*N*,*N*′,*N*′-tetramethyl-1,4-phenylenediamine (TMPD), and 4-nitrothiophenol (4-NTP) in dimethyl sulfoxide (DMSO) were mixed thoroughly with the aqueous nanoparticle solutions in order to obtain final concentrations of up to 100 μM. Thus, the DMSO concentration in the nanoparticle solution does not exceed 0.1% v/v. DMSO concentrations greater than 5% v/v destabilize silver nanoparticle solutions by dissolving the silver cores.[30] DMSO was used as transfer agent for the functionalizing compounds into the aqueous phase of the nanoparticle solution, where neutral TCNQ and 4-NTP are otherwise insoluble. TCNQ forms a protecting shell around nanoparticles, whereas TMPD acts as a cross-linking agent. Ones modified with TCNQ or 4-NTP subsequent addition of typical fast-reacting cross-linking agents such as dithiols in even concentration ratios compared to the functionalizing agents are not leading to an otherwise immediate aggregation of the nanoparticles. This would be clearly visible by a color change from reddish to blue-purple in the case of the gold nanopaticles and from yellow to brown in the case of the silver nanoparticles. The exchange of TCNQ or 4-NTP with such dithiols followed by aggregation of the nanoparticles occurs only at a time scale of several hours. It shows that at least one dense monolayer has been established on the nanoparticle surface. In contrast, the addition of lower concentrations (1 nM to 1 μM) of TMPD leads to an instantaneous color change followed by a slow, in the order of hours, sedimentation of built aggregates. Such aggregates are too large to be useful in the further described experiments. Using high concentrations of TMPD of up to 100 μM together with ultrasonic activation, the developing aggregates can be limited in their growth. As soon as all free surfaces of the cross-linking metallic nanoparticles are covered with TMPD, further aggregation ceases. Such size-limited nanoparticle aggregates precipitate in a time scale of several days and not hours. The functionalized nanoparticle solutions were centrifuged at 20 000*g* until a pellet or concentrate and a supernatant had formed. The pellet or concentrate was resuspended using ultrasound. Two or three washing steps followed, consisting of adding fresh solvent (in this case water), vortexing, and subsequently centrifuging. This procedure removed impurities such as salts which arise from the nanoparticle synthesis and any excess of the functionalizing molecules. The final concentrate had a metal content of up to 100 mg/mL. The concentrations were measured by using spectrophotometry, assuming the absorbance spectra had not changed due to irreversible aggregation. Alternatively, volumetric ratios were used to calculate the concentration factor when all nanoparticles were transferred into the concentrate without observable losses on tube walls. Each method was checked beforehand by elemental microanalysis of the metals using atomic emission spectroscopy.

2.2. Formation of Functionalized Nanoparticle Film. The functionalized nanoparticle concentrates were used in a manner similar to conventional inks in a double action Iwata HP-A airbrush (Medea Airbrush Products, Portland, OR). The films were sprayed on highly ordered pyrolytic graphite (HOPG from Structure Probe, Inc., USA). Samples were made on nonconductive printer transparency film (Seiko Epson Corporation, USA, Japan). During the deposition, patterning of the nanoparticle films was achieved by using shadow masks (Photo Chemical Machining by Mastercut Technologies, Australia). Thus, structures could be made with clearly defined, stepped edges. The volume of the concentrate used and the deposition area allowed the determination of the approximate film thicknesses using eq 1:

$$d = \frac{(r_c + l_f)^3 V_c}{f_p r_c^3 A_f} \quad (1)$$

where d is the film thickness, r_c is the core radius, l_f is the thickness of the functionalizing layer assuming a single length of the functionalizing molecule, V_c is the volume of all deposited nanoparticle cores, A_f is the film area, and f_p is the volume fraction of 3-D packed spheres. We assume a dense face-centered-cubic lattice packing with an f_p of 0.74. Due to the irregularities in the nanoparticle packing, the void fraction will be higher and the calculated film thickness thus represents a lower limit. The thicknesses of the deposited functionalized nanoparticle films were between 100 and 200 nm, which means each film had between 12 and 25 layers of 10 nm silver nanoparticles or between 8 and 17 layers of 15 nm gold nanoparticles. Although, each of these nanoparticle films is essentially a multilayer, we define structures made out of two nanoparticle films as bilayers.

2.3. Characterization. For the measurement of resistivities the nanoparticle films were connected by copper wire electrodes in a two-probe configuration using silver paint. Resistance values of the nanoparticle films were obtained by applying a voltage and measuring the current with an AdInstruments Pty. Ltd. potentiostat. Scanning electron micrographs were taken using a Gemini 1550 SEM (OMICRON NanoTechnology GmbH, Germany). The electron tunneling experiments were carried out under ambient conditions on an easyScan STM (Nanosurf AG, Switzerland) using Pt−Ir tips. Each of the scanning tunneling spectroscopy (STS) curves consisted of an average obtained

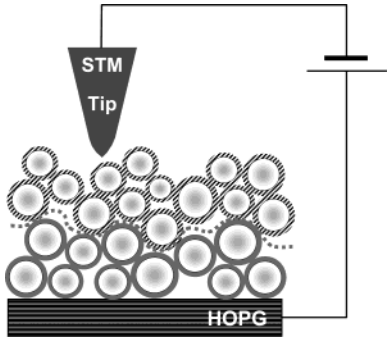

Figure 1. Schematic picture of the studied nanostructure with lower nanoparticle film, hetero-molecular interface (dotted line), and upper nanoparticle film between HOPG substrate and Pt−Ir tip. The nanoparticle cores are of the same material, the different functionalizing shells around them are indicated in gray and diagonal-striped patterns. In the following figures, nanoparticle films functionalized with electron acceptors are labeled with A, whereas functionalizations with electron donors are labeled with D.

from 50 spectra to improve the signal-to-noise ratio. The voltage is measured between the tip and the substrate, where the substrate is grounded and herewith on zero electrostatic potential. The $I(V)$ data in Figures 4a, 5a, 7a, 8a, and 9a were fitted with an exponential decay plus growth function of the type

$$I = I_0 + I_1 \exp(-V/V_1) + I_2 \exp(V/V_2) \qquad (2)$$

where I_0, I_1, I_2, V_1, and V_2 are constants, to smooth the steps which occurred through the digital generation of the voltage ramp before the first derivative dI/dV was calculated. For the data in Figure 6a, we used five data points adjacent averaging. Together with the original $I(V)$ data shown in gray, all fitting or smoothing curves are displayed as black hairlines. The dI/dV curves are shown again in gray together with their fitting curves in black.

The nanostructure under study is schematically shown in Figure 1.

3. Results and Discussion

Composite thin films consisting of metallic nanoparticles which were modified using organic molecules were formed through spray deposition of aqueous concentrates. Depending on the compounds and the concentration ratios used, the functionalizing agents will act as spacers or will partially modify the surfaces allowing the metallic nanoparticle cores in the film to touch each other.

Figure 2 shows the surface topography of a film of silver nanoparticles which were functionalized by the redox-active compound 4-NTP.[31] Here the nanoparticles have an average diameter of 80 nm allowing easy imaging. The figure illustrates the disordered but nevertheless densely packed structure of nanoparticle films achieved by the method of spray deposition. The particles did not assemble into ordered super lattices and formed a rather irregular network of varying void sizes. The silver and gold nanoparticles used in the following STS studies were 10 and 15 nm in diameter.

Figure 3 shows one example of STM images of functionalized nanoparticle films. Like the previous SEM micrograph (Figure 1), it shows a disordered but dense nanoparticle structure. Figure 3 demonstrates that it is possible to perform STM work on films that are 8 to 17 nanoparticles thick.

A nanoparticle film can be viewed as a multi-junction system where the junctions are the molecular bridges between adjacent

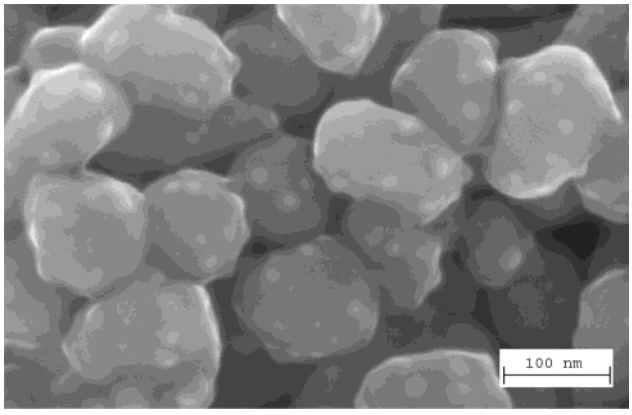

Figure 2. Scanning electron micrograph of the surface of a spray-deposited silver nanoparticle (core)/4-NTP (shell) film. The silver nanoparticles have an average diameter of 80 nm.

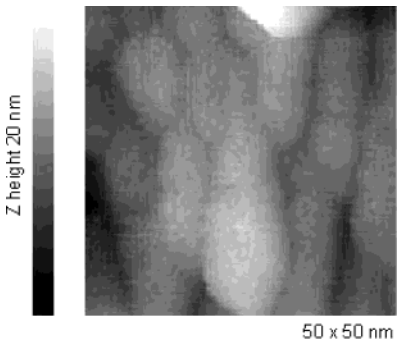

Figure 3. STM image at V_{bias} = 50 mV, I_{set} = 1 nA of a spray-deposited gold nanoparticles (core)/TCNQ (shell) film on HOPG. The gold nanoparticles have an average diameter of 15 nm.

nanoparticles. The STS experiment measures the dependence of tunneling currents through the multi-junction system as a function of the applied voltage ($I(V)$). Due to geometric constrains, we could not measure the characteristic of a bilayer via direct, electrical (silver paint, physical vapor deposition of metals) contacts to each layer. Using eq 1 to determine the film thicknesses, the resistivities of the film materials range from 10^{-7} to 10^{-4} Ω m. A 1 mm^2 area of 200 nm thickness shows longitudinal resistance between 0.32 Ω and 320 Ω, whereas the transverse resistance is as low as 2×10^{-8} Ω or 2×10^{-5} Ω, respectively, when we assume that the transverse resistivity is the same as the measured longitudinal resistivity. As the longitudinal conduction along uniform functionalized nanoparticle films can be described by percolation theory,[32] this might be not correct when characteristic cluster lengths become larger than the film thickness itself. However, all measurements taken gave extremely low resistances, and could not be differentiated from short circuit conditions. In long, flat successive films with a bilayer formed at the contact between films, most of the applied voltage drops off along the connecting nanoparticle film and not along the interface. On the other hand, thin bilayer structures which are directly connected on the top and bottom exceed current limits of the measurement equipment at even very low applied voltages. The STM allows the probing of thin layered structures over a wide voltage range with subnanometer resolution.

The $I(V)$ behavior for the HOPG substrate was first evaluated and found to be very similar to that reported previously.[33,34]

First, we investigated the $I(V)$ characteristic of homogenic functionalized nanoparticle films on HOPG for 10 nm silver nanoparticle−TCNQ as shown in Figure 4 and for 10 nm silver

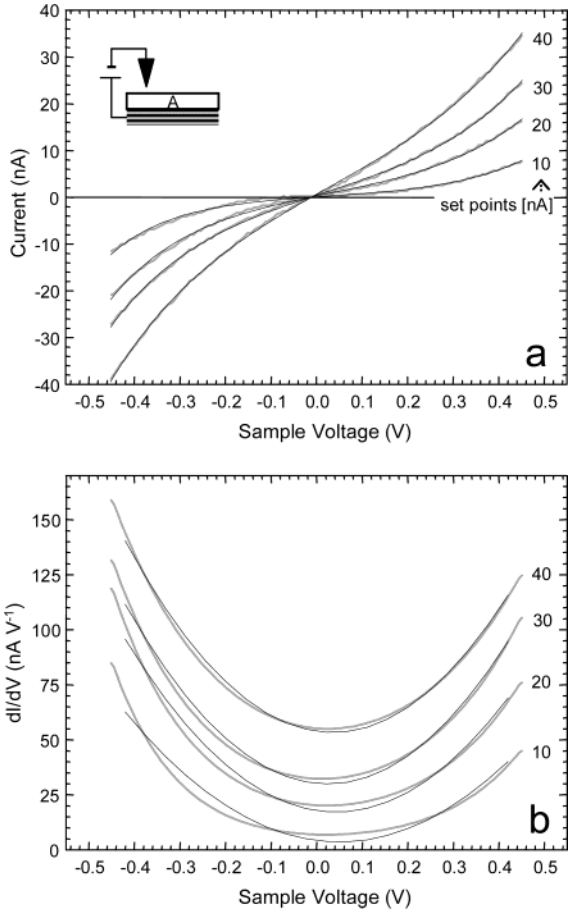

Figure 4. (a) The current vs voltage and (b) the differential conductance vs voltage constant-height mode tunneling spectroscopy data of a 10 nm pure silver nanoparticle−TCNQ film on HOPG. The tip position was changed through different set points at a fixed voltage of 0.5 V. The inset schematically depicts the structure under investigation.

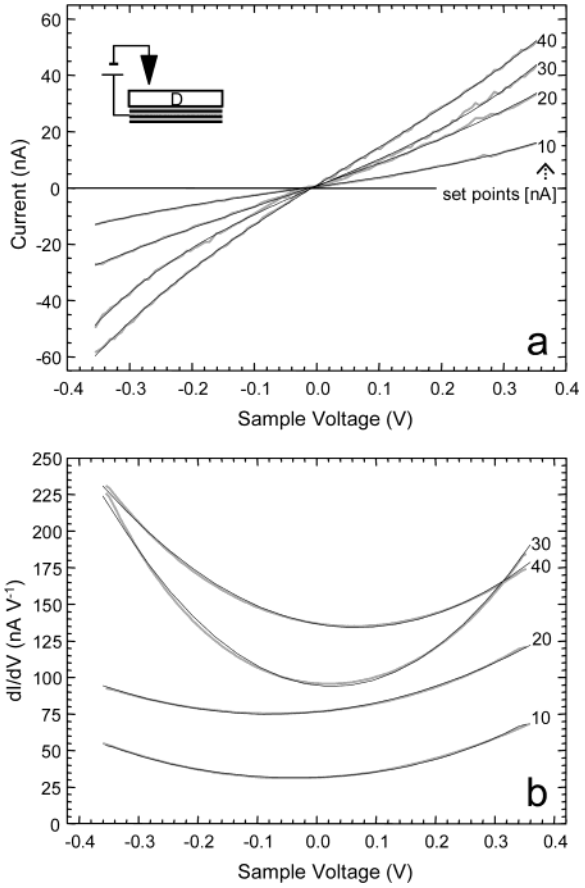

Figure 5. (a) The current vs voltage and (b) the differential conductance vs voltage constant-height mode tunneling spectroscopy data of a 10 nm pure silver nanoparticle−TMPD film on HOPG. The tip position was changed through different set points at a fixed voltage of 0.3 V.

nanoparticle−TMPD as shown in Figure 5. The spectra are symmetric as expected, and their shape is approximately conserved on varying the tip−sample separation. Because of the relatively low voltage range ($< \pm 1$ V), the differential conductance dI/dV in our multi-junction systems is approximately parabolic as is predicted for metal−insulator−metal junctions.[35] The shape of the curves changed little with variations of the set point according to the height of the tip above the substrate. For the 10 nm silver nanoparticle−TCNQ film of Figure 4b, the parabolic fits improve as the tip approaches the film surface. All fits display a negative linear term representing a steeper current increase at negative voltages. The differential conductivities dI/dV of the 10 nm silver nanoparticle−TMPD film (Figure 5b) are all qualitatively similar. The parabolic fits start with a positive linear term when the tip is farther away from the surface which becomes negative on approaching the surface. Variations of the tip height should affect the ratio of the voltage drop within the tunnel junctions of the nanoparticle film and the single tunnel junction between the film and the tip. Overall, fitted coefficients for the quadratic term for each film start at around 250 nA V^{-3} and increases to 500 nA V^{-3} as the gap to the surface narrows, except at the set point of 30 nA in Figure 5b.

Second, we investigated bilayer structures of functionalized nanoparticle films in which either the electron acceptor (A) or the electron donor (D) layer was first deposited nearest to the substrate. The STS data in Figure 6 clearly show diode-like behavior where under forward voltage conditions the configuration is always cathode → A → D → anode. This corresponds to an electron flux along the arrows shown above.

Under reverse voltage conditions, STS studies on both bilayer structures show near zero differential conductivity. Under forward voltage conditions, the magnitude of the current increases linearly with the applied voltage for the A−D and the D−A structure. The knee in the $I(V)$ curve for the HOPG−D−A $I(V)$ curve lies at a threshold voltage of 0 V, whereas the knee for the HOPG−A−D $I(V)$ curve is shifted toward a threshold voltage of −100 mV, followed by a current offset of −30 nA. The rectification ratio is defined as the ratio of the currents under forward and reverse voltage conditions. The rectification ratios are 2.2 at ±250 mV and 66 at ±75 mV for HOPG−A−D and HOPG−D−A, respectively.

Similar asymmetric interfaces have been created using a second nanoparticle system. Gold nanoparticles with an average diameter of 15 nm were used to produce layered HOPG−A−D (Figure 7) and reverse HOPG−D−A (Figure 8) structures. Even though the transition between forward and reverse voltage conditions is not as sharp as it is in the case of the silver nanoparticle samples, the STS measurements show a highly asymmetric $I(V)$ behavior which can be fitted using eq 2 in order to obtain the differential conductance. The rectification ratios are 6.5 at ±1 V for the HOPG−A−D structure and 4 at ±1 V for the HOPG−D−A structure. Figure 9 compares representative curves for each structure. The spectra overlap at a voltage range between 0 and 80 mV due to a current offset of around 10 nA of the HOPG−D−A sample.

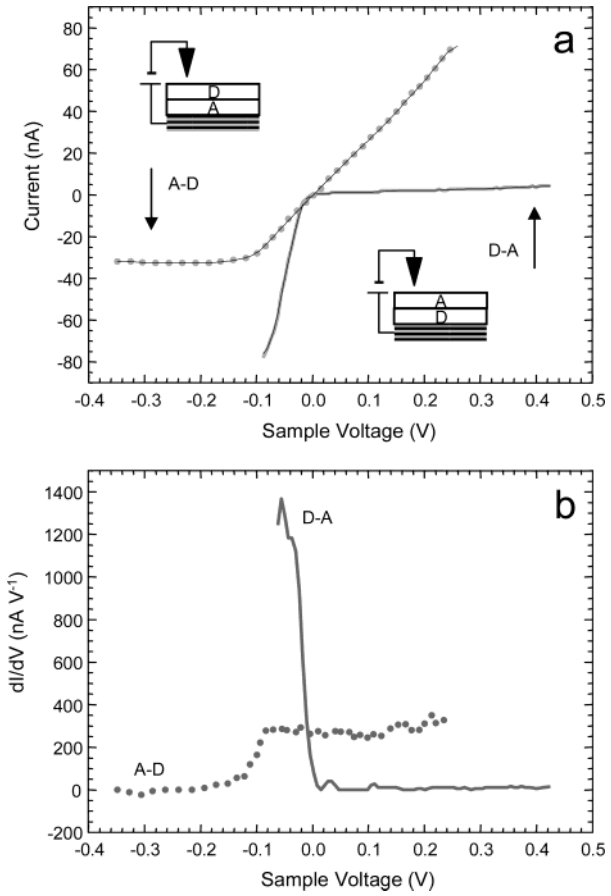

Figure 6. (a) The current vs voltage and (b) the differential conductance vs voltage tunneling spectroscopy data of 10 nm silver nanoparticle bilayers on HOPG. The tip position above the HOPG−D−A structure was fixed through a set point of 1 nA at a bias voltage of 0.1 V and above the HOPG−A−D structure through a set point of 1 nA at a bias voltage of 0.2 V. The insets show schematically the structures under investigation.

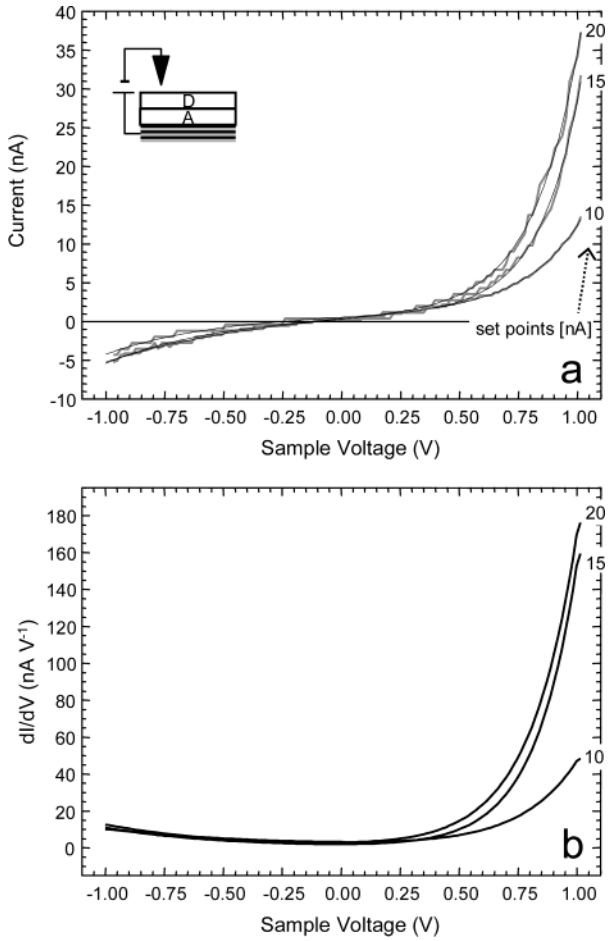

Figure 7. (a) The current vs voltage and (b) the differential conductance vs voltage constant-height mode tunneling spectroscopy data of 15 nm gold nanoparticle bilayers with the orientation HOPG−A−D. The tip position was changed through different set points at a fixed bias voltage of 1 V. The inset shows schematically the structure under investigation.

Models for the Rectifying Nanoparticle Structures. The rectifying behavior observed in these bilayer structures can be described qualitatively by two models: (Model A) treating the metal nanoparticles as a supporting and connecting matrix, and (Model B) the possibility of a Schottky contact mechanism. These two models are now discussed.

Model A. Model A is based on the Aviram and Ratner approach.[1] Here, we treat the metal nanoparticles as a supporting and connecting matrix. The diode-like behavior is thought to be caused by the asymmetric TCNQ−TMPD interface. In the model of Aviram and Ratner, the highest occupied molecular orbital (HOMO) levels of isolated typical electron donors are in the range of −6 to −9 eV, the lowest unoccupied molecular orbital (LUMO) levels of isolated typical electron acceptors are in the range −1 to −2.5 eV. Thus, the differences between them are at least 3.5 eV. Through the interactions with the electronic states of the connecting electrodes, the energy levels of the molecules shift so that the difference between D−HOMO and A−LUMO becomes less than several hundred meV. The $I(V)$ characteristic for an A−D bilayer is a step function showing a threshold voltage of several hundred millivolts under forward voltage conditions (cathode → A → D → anode). The threshold voltage is caused by the voltage which is necessary to align the cathode Fermi levels with A−LUMO as well as the anode Fermi levels with D−HOMO. At and above the threshold voltage, resonance tunneling occurs at the cathode/A−LUMO interface and at the anode/D−HOMO interface. The $I(V)$ characteristic for the reverse voltage essentially represents the off-resonance tunneling current through an insulating layer with a thickness of the A and D molecules together. In our case, we calculate the energies of the electron donor TMPD to be −7.67 eV for the HOMO and 0.77 eV for the LUMO level using the semiempirical PM3 method which is provided by the program CS Chem 3D pro (CambridgeSoft, Cambridge, USA). Beforehand, the molecular structures underwent a geometry optimization using the molecular mechanics MM2 algorithm from the same program. The corresponding values for the electron acceptor TCNQ are −9.55 eV and −2.92 eV. These values are within the range of Aviram and Ratner's A and D energy levels. We could not observe a step function. However, our results show distinct asymmetric $I(V)$ characteristics for all gold and silver nanoparticle bilayer structures. A broadening of the knee in the $I(V)$ curve at a relatively large threshold voltage of around 0.75 V has been found for the gold nanoparticle (Figure 7). The threshold voltage can be estimated from a linear approximation of the last few data points of each measurement. These $I(V)$ curves and their fits with exponential curves are similar to published results for LB-films of zwitterionic $D^+-\pi-A^-$ compounds. Monolayers[3] and films of up to 4 layers[36] sandwiched between metal electrodes showed $I(V)$ characteristics which were readily fitted by $I = a \exp(bV)$ for a single quadrant.[2] Metzger et al. reviewed four other models without finding significant better fits to their $I(V)$ curves which were

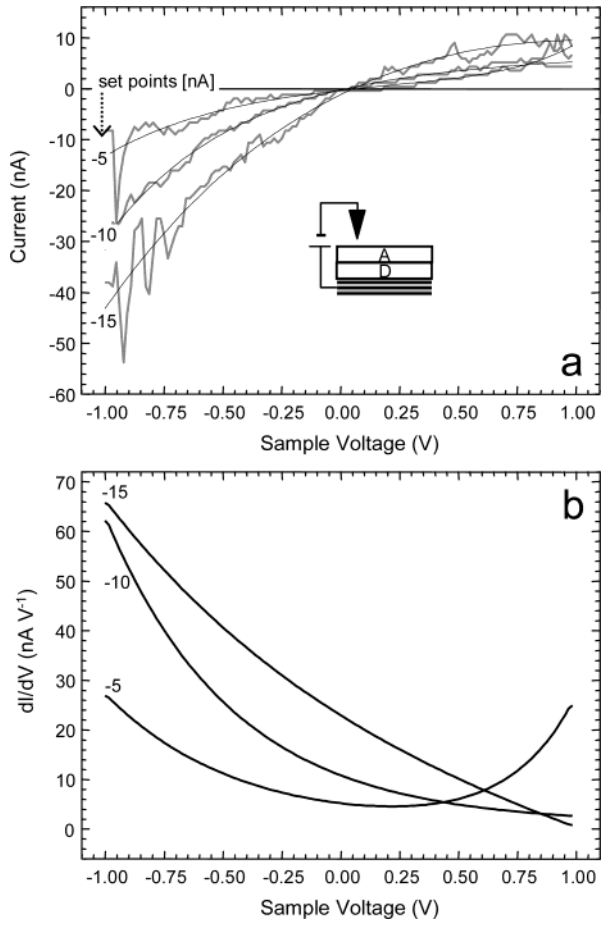

Figure 8. (a) The current vs voltage and (b) the differential conductance vs voltage constant-height mode tunneling spectroscopy data of 15 nm gold nanoparticle bilayers with the HOPG−D−A orientation. The tip position was changed through different set points at a fixed bias voltage of −0.5 V.

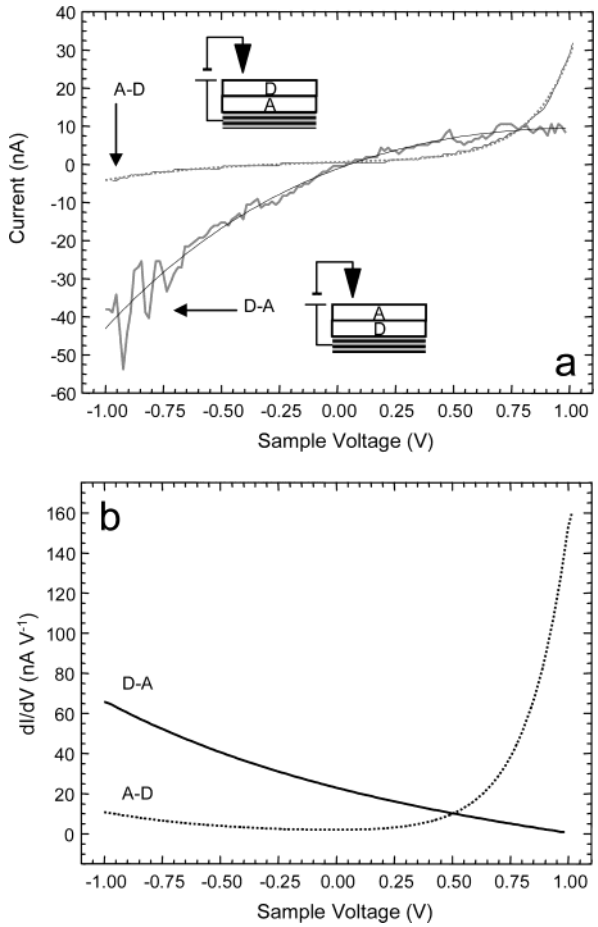

Figure 9. (a) The current vs voltage and (b) the differential conductance vs voltage tunneling spectroscopy data of 15 nm gold nanoparticle bilayer on HOPG. The tip position for the HOPG−D−A structure was fixed through a set point of 15 nA at a bias voltage of 1 V and at the HOPG−A−D structure through a set point of −15 nA at a bias voltage of −0.5 V. The insets show schematically the structures under investigation.

taken from a hexadecylquinolinium tricyanoquinodimethanide monolayer sandwiched between gold electrodes.[37]

A sharp transition occurs between forward and reverse voltage conditions for the silver nanoparticle samples. We observed an abrupt change from almost no increase in current to a linear current increase, which is atypical for known diode *I*(*V*) characteristics. Nevertheless, similar behavior has been observed in zwitterion multilayers of the type Au/100 LB layers/Au,[6] where it was proposed that the shape of the *I*(*V*) curve might result from field-induced realignment of the zwitterionic molecules within the multilayer structure. Although each nanoparticle film consists of many nanoparticle layers, the asymmetry of the bilayer film structure and consequently of the *I*(*V*) curve is caused in our case only by one A−D heteromolecular interface. Brought together, A and D molecules form in solution A^-D^+ charge transfer complexes which we similarly expect to become formed at a dry interface. The A^-D^+ interface between the two nanoparticle films is rough. The electronic properties of each A^-D^+ charge-transfer complex are influenced by different local geometric configurations and environments. This might create the observed ohmic molecular conductor under forward voltage conditions analogous to a sequential stack of A and D molecules in molecular conductors.[38,39] We did mention earlier, the Aviram and Ratner model predicts that under reverse voltage conditions the orbital levels shift in the opposite direction, pulling them further apart. This leads to an off-resonance tunneling gap of essentially the length of A plus D, in our case ca. 1.2 nm, along the A−D interface which determines from hereon the *I*(*V*) characteristic. Charge-transfer complexes are characterized through an intermolecular electron transfer, which establishes an internal electric field across the interface between A^- and D^+. This might cause the shift in the threshold voltage and cause the constant current at further negative potentials which we observed in the *I*(*V*) curve of the silver nanoparticle HOPG−A−D structure in Figure 6a. Unfortunately, we were not able to produce mirror-image *I*(*V*) curves by inverting the D−A order. The formation of the interfaces is subject to several processes such as wetting and drying, alignment, and interlocking of the nanoparticles as well as the surface-attached molecules. We did observe small changes in the film formation and its appearance, depending on the order of the deposition. This could explain the differences between the HOPG−D−A and HOPG−A−D samples (Figure 6).

Model B. In this model we consider the possibility of a Schottky contact mechanism. Schottky diodes are formed by junctions between metals and doped semiconductor materials. In the case of a metal p-semiconductor junction, only at Fermi-level relations $\Phi_{metal} < \Phi_{semiconductor}$ we would have rectifying contacts otherwise ohmic contacts. The forward voltage condition for the rectifier is given by cathode → (metal) → (p-semiconductor) → anode. Present, the $A_{(TCNQ)}$-modified nanoparticle films have lower resistivities than the comparable

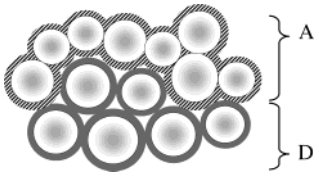

Figure 10. Illustration of nanoparticle films with different surface densities of the functionalizing agent.

$D_{(TMPD)}$-modified ones, so they behave more as metals in their conduction properties. The A−gold nanoparticle film has a resistivity of 3×10^{-7} Ω m, while the A−silver nanoparticle films have a value of 2.15×10^{-7} Ω m. The D−gold nanoparticle film has a resistivity of 5.7×10^{-4} Ω m, while the D−silver nanoparticle films have a value of 3.75×10^{-6} Ω m. This means that the A-functionalized side reveals resistivities which are only one magnitude higher than for the pure bulk metal. If we take into consideration that voids reduce the effective internal cross-section, we can describe the A−nanoparticle films as highly porous metallic films modified with A−molecules along the inner surface. The particle cores are touching each other, forming a metallic scaffold. Alternatively, the D-functionalized sides contain insulated nanoparticle cores with a thoroughly thermally activated tunneling conduction mechanism.[40] Since the observed forward voltage in our examples is along the cathode → (A) → (D) → anode direction, it could be written in this context as cathode → ("metallic") → ("p") → anode. This is exactly the forward voltage direction of a cathode → (metal) → (p-semiconductor) → anode Schottky-diode.

Model B raises the question of how it is possible that a molecular interface separates both films, whereas the particles in one of the films are physically touching each other. We have to bear in mind that if the nanoparticle surfaces are not completely covered with functionalizing organic molecules, the particle cores may form contacts while similar molecules may repel each other and change their position at the particle surface during the film deposition (Figure 10 layer A). At the interface between two films the conditions are different. The functionalizing molecules A and D attract each other, especially as they form A^-D^+ charge-transfer complexes. During the film deposition, these processes might guide the formation of a stable hetero-molecular interface between the nanoparticle films, even if one film does not form dense molecular barriers between all of its nanoparticle cores (Figure 10).

The presented experiments could proof the qualitative similarity in $I(V)$ characteristics of the silver and gold nanoparticle bilayer structures. However, there are obvious differences in the shape of the curves. On one hand, we have used different sized nanoparticles, 10 nm for the silver and 15 nm for the gold samples, and the resulting films display the above-mentioned different resistivity values. On the other hand, the formation of the organic shells might vary, depending on the chosen metal core. Silver interacts when in contact with neutral TCNQ, and Ag^+TCNQ^- salt is formed on the surface.[41] Ag^+TCNQ^-, like the corresponding copper(I/II) salts, shows electrical field-induced phase transitions.[42] The resistivity of these salts switches from a high impedance state to a low impedance state by applying an electric field. The formation of Au^+TCNQ^- salt with similar behavior has not been reported yet, even if spontaneous open circuit reduction of yellow TCNQ to blue $TCNQ^-$(aq) on bulk gold occurs in various aqueous electrolytes.[43] This might be caused by transfer of excess charges and not through aurous formation.

4. Conclusion

In conclusion, rectifying current−voltage characteristics have been observed for asymmetric interfaces between nanoparticles which have been functionalized with electron acceptors and electron donors. Instead of synthesizing D−bridge−A−anchor molecules, aligning them in LB-films and transferring them onto solid substrates or developing systems capable of self-assembly, we spray-deposited successive D- and A-components directly onto the substrate. Metal nanoparticle cores act as a stabilizing and conducting matrix. Both models proposed describe qualitatively the rectifying behavior which we observed in these functionalized nanoparticles layers. To further clarify the origin of the rectifying behavior, we propose systematic experiments with different nanoparticle functionalizing D- and A-compounds.

Acknowledgment. We acknowledge A. Wilson and P. Vincent from Defence Science and Technology Organization, Australia, for taking the electron micrographs and S. Lavrencic from the Centre for Advanced Analytical Chemistry at CSIRO Energy Technology for undertaking the microanalyses. We thank Karl-Heinz Müller, Burkhard Raguse, and Scott Martin for the fruitful and inspiring discussions. Financial support from the Australian Research Council is gratefully acknowledged.

References and Notes

(1) Aviram, A.; Ratner, M. A. *Chem. Phys. Lett.* **1974**, *29*, 277.
(2) Ashwell, G. J.; Sambles, J. R.; Martin, A. S.; Parker, W. G.; Szablewski, M. *J. Chem. Soc.−Chem. Commun.* **1990**, *19*, 1374.
(3) Martin, A. S.; Sambles, J. R.; Ashwell, G. J. *Phys. Rev. Lett.* **1993**, *70*, 218.
(4) Metzger, R. M.; Chen, B.; Hopfner, U.; Lakshmikantham, M. V.; Vuillaume, D.; Kawai, T.; Wu, X. L.; Tachibana, H.; Hughes, T. V.; Sakurai, H.; Baldwin, J. W.; Hosch, C.; Cava, M. P.; Brehmer, L.; Ashwell, G. J. *J. Am. Chem. Soc.* **1997**, *119*, 10455.
(5) Metzger, R. M. *Synth. Met.* **2001**, *124*, 107.
(6) Ashwell, G. J.; Gandolfo, D. S. *J. Mater. Chem.* **2001**, *11*, 246.
(7) Ashwell, G. J.; Gandolfo, D. S.; Hamilton, R. *J. Mater. Chem.* **2002**, *12*, 416.
(8) Ashwell, G. J.; Gandolfo, D. S. *J. Mater. Chem.* **2002**, *12*, 411.
(9) Baldwin, J. W.; Amaresh, R. R.; Peterson, I. R.; Shumate, W. J.; Cava, M. P.; Amiri, M. A.; Hamilton, R.; Ashwell, G. J.; Metzger, R. M. *J. Phys. Chem. B* **2002**, *106*, 12158.
(10) Ashwell, G. J.; Paxton, G. A. N. *Aust. J. Chem.* **2002**, *55*, 199.
(11) Okazaki, N.; Sambles J. R.; Jory, M. J.; Ashwell, G. J. *Appl. Phys. Lett.* **2002**, *81*, 2300.
(12) Metzger, R. M.; Baldwin, J. W.; Shumate, W. J.; Peterson, I. R.; Mani, P.; Mankey, G. J.; Morris, T.; Szulczewski, G.; Bosi, S.; Prato, M.; Commito, A.; Rubin, Y. *J. Phys. Chem. B* **2003**, *107*, 1021.
(13) Reichert, J.; Ochs, R.; Beckmann, D.; Weber, H. B.; Mayor, M.; von Lohneysen, H. *Phys. Rev. Lett.* **2002**, *88*, 176804.
(14) Chen, J.; Reed, M. A.; Rawlett, A. M.; Tour, J. M. *Science* **1999**, *286*, 1550.
(15) Pope, M.; Swenber, C. E. *Electronic Processes in Organic Crystals and Polymers*; Oxford University Press: Oxford, 1999.
(16) Garnier, F.; Hajlaoui, R.; Yassar, A.; Srivastava, P. *Science* **1994**, *265*, 1684.
(17) Patel, N. K.; Cina, S.; Burroughes, J. H. *IEEE J. Sel. Top. Quantum Electron.* **2002**, *8*, 346.
(18) Fischer, C. M.; Burghard, M.; Roth, S. *Synth. Met.* **1995**, *71*, 1975.
(19) Fischer, C. M.; Burghard, M.; Roth, S.; von Klitzing, K. *Surf. Sci.* **1996**, *362*, 905.
(20) Chabinyc, M. L.; Chen, X. X.; Holmlin, R. E.; Jacobs, H.; Skulason, H.; Frisbie, C. D.; Mujica, V.; Ratner, M. A.; Rampi, M. A.; Whitesides, G. M. *J. Am. Chem. Soc.* **2002**, *124*, 11730.
(21) McConnell, W. P.; Novak, J. P.; Brousseau, L. C.; Fuierer, R. R.; Tenent, R. C.; Feldheim, D. L. *J. Phys. Chem. B* **2000**, *104*, 8925.
(22) Uosaki, K. *Electrochemistry* **1999**, *67*, 1105.
(23) Martin, J. E.; Wilcoxon, J. P.; Odinek, J.; Provencio, P. *J. Phys. Chem. B* **2000**, *104*, 9475.
(24) He, H. X.; Zhang, H.; Li, Q. G.; Zhu, T.; Li, S. F. Y.; Liu, Z. F. *Langmuir* **2000**, *16*, 3846.
(25) Fuller, S. B.; Wilhelm, E. J.; Jacobson J. M. *J. Microelectromech. Syst.* **2002**, *11*, 54.

(26) Turkevich, J.; Stevenson, P. C.; Hillier, J. *Discuss. Faraday Soc.* **1951**, *11*, 55.
(27) Frens, G. *Nature Phys. Sci.* **1973**, *241*, 20.
(28) Creighton, J. A.; Blatchford, G. C.; Albrecht, M. G. *J. Chem. Soc., Faraday Trans. 2* **1979**, *75*, 790.
(29) Lee, P. C.; Meisel, D. P. *J. Phys. Chem.* **1982**, *86*, 3391.
(30) Rodriguez-Gattorno, G.; Diaz, D.; Rendon, L.; Hernandez-Segura, G. O. *J. Phys. Chem. B* **2002**, *106*, 2482.
(31) Tsutsumi, H.; Furumoto, S.; Morita, M.; Matsuda, Y. *J. Colloid Interface Sci.* **1995**, *71*, 505.
(32) Müller, K. H.; Herrmann. J.; Raguse, B.; Baxter, G.; Reda, T. *Phys. Rev. B* **2002**, *66*, 075417.
(33) Klusek, Z. *Appl. Surf. Sci.* **1997**, *108*, 405.
(34) Colton, R. J.; Baker, S. M.; Driscoll, R. J.; Younquist, M. G.; Baldeschwieler, J. D.; Kaiser, W. J. *J. Vac. Sci. Technol. A* **1988**, *6*, 349.
(35) Lambe, J.; Jaklevic, R. C. *Phys. Rev.* **1968**, *165*, 821.
(36) Metzger, R. M. *J. Mater. Chem.* **2000**, *10*, 55.
(37) Metzger, R. M.; Xu, T.; Peterson, I. R. *J. Phys. Chem. B* **2001**, *105*, 7280.
(38) Caro, J.; Fraxedas, J.; Figueras, A. *Chem. Vapor Deposition* **1997**, *3*, 263.
(39) Nakamura, T.; Isotalo. H.; Akutagawa, T.; Tachibana, H.; Azumi, R.; Matsumoto, M.; Horiuchi, S.; Yamochi, H.; Saito, G. *Thin Solid Films* **1996**, *285*, 508.
(40) Raguse, B.; Herrmann, J.; Stevens, G.; Myers, J.; Baxter, G.; Müller, K. H.; Reda, T.; Molodyk, A.; Braach-Maksvytis, V. J. *Nanoparticle Res.* **2002**, *4*, 137.
(41) O'Kane, S. A.; Clerac, R.; Zhao, H. H.; Xiang, O. Y.; Galan-Mascaros, J. R.; Heintz, R.; Dunbar, K. R. *J. Solid State Chem.* **2000**, *152*, 159.
(42) Potember, R. S.; Poehler, T. O.; Cowan, D. O. *Appl. Phys. Lett.* **1979**, *34*, 405.
(43) Snook, G. Investigation of Solid-State Reactions by Electrochemical and Quartz Crystal Microbalance Measurements. Ph.D. Thesis, Dept. of Chemistry, Monash University, Melbourne, Australia, 2000.